# Prediction of flashback limits for laminar premixed hydrogen-air flames using flamelet generated manifolds

Available online at www.sciencedirect.com

ScienceDirect

journal homepage: www.elsevier.com/locate/he

# Prediction of flashback limits for laminar premixed hydrogen-air flames using flamelet generated manifolds

F.H. Vance [a,b,*], L.P.H. de Goey [b], J.A. van Oijen [b,c]

[a] Simulation of Reactive Thermo-Fluid Systems, TU Darmstadt, Germany
[b] Mechanical Engineering, Eindhoven University of Technology, Eindhoven, the Netherlands
[c] Eindhoven Institute for Renewable Energy Systems, Eindhoven University of Technology, Eindhoven, the Netherlands

## HIGHLIGHTS

- First study with estimation of flashback limits with flamelet generated manifolds.
- Flashback limits for methane-air flames are predicted in a good manner.
- Hydrogen flashback limits are over-predicted with a 3D manifold.
- The difference is caused by enthalpy gradients across thick reaction zone.
- A simple correction model is proposed which improves the model for hydrogen flames.

## GRAPHICAL ABSTRACT

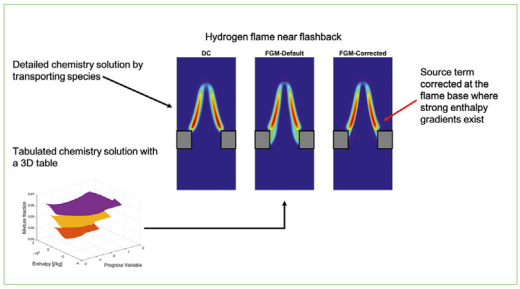


## ARTICLE INFO

*Article history:*
Received 10 December 2022
Received in revised form
9 March 2023
Accepted 18 March 2023
Available online 12 April 2023

*Keywords:*
Hydrogen
Flashback
Thick reaction zone
Heat loss
Flamelet generated manifolds

## ABSTRACT

Development of models that can help predict flashback limits of premixed flames at an affordable computational cost is essential for the safe and efficient design of combustion chambers. For flames with strong preferential diffusion effects, usually the focus has been on the development of at least a three dimensional flamelet database that can predict the enthalpy and mixture fraction mapped on to the reaction progress variable. However, in this study, we show that a 3D FGM table is sufficient to predict flashback limits for lean laminar methane-air flames but is not sufficient to predict the same for lean hydrogen flames and an over-prediction of 100% could occur in the calculation of the flashback limits. We trace the root cause of this over-prediction to be related to the thickness of the reaction zone in the progress variable for hydrogen flames. This results in the development of a novel correction factor for the progress variable source term using 1D flame simulations where the flame experiences strong enthalpy gradients. In the end, we successfully

* *Corresponding author*. Simulation of Reactive Thermo-Fluid Systems, TU Darmstadt, Germany.
E-mail address: vance@stfs.tu-darmstadt.de (F.H. Vance).

https://doi.org/10.1016/j.ijhydene.2023.03.262

show for the first time that the flashback limits for hydrogen flames can be predicted accurately using flamelet generated manifolds with a source term corrector function.


## Introduction

Combustion of natural gas results in emission of $CO_2$ which can harm the environment. Replacing natural gas with hydrogen could pave the way for cleaner generation of power and heat. However, a hydrogen flame has significant differences with a methane flame especially related to the stabilization behaviour. The flame speed of hydrogen is significantly higher than that of methane's while the low Lewis number of hydrogen compared to methane can cause the hydrogen flame to burn stronger for conditions for which a methane flame burns weaker. These differences could lead to significant problems such as flashback, which occurs as the flame speed of a premixed flame exceeds the flow velocity, causing the flame to move upstream of flame anchoring devices [1–3]. Flashback can cause considerable damage to the burner and upstream equipment. For methane, flame's propensity to flashback is smaller than that for hydrogen flames due to latter's higher flame speed coupled with preferential diffusion effects [4]. The prediction of flashback limits using reduced methods at an affordable computational cost is essential for safe design of combustion chambers for both domestic and commercial devices. Although hydrogen chemical mechanisms have less number of species than hydrocarbons, the prediction of flame dynamics using reduced methods such as flamelet generated manifolds [5] is still essential for the design and analysis of hydrogen burners for small and large scale combustors. Development of such models for pure $H_2$-air or $H_2$ dominated fuels has attracted much attention in the past few years with most of the models usually employing a three dimensional flamelet database with progress variable, enthalpy and a mixture fraction to capture heat transfer, stretch and curvature effects [6–19].

Previous studies on flame stabilization in laminar premixed flames have shown that conjugate heat transfer between the flame and the burner is important for accurate prediction of flame anchoring [20–25] and flashback and blow-off limits [3,26,27]. Investigations have also been made into different aspects of hydrogen combustion [1,2,28–36]. Flames near the flashback limit usually stabilize closer to the burner and are also impacted by flame stretch. For hydrogen flames, positive flame stretch induces strong preferential diffusion effects which enhance the flame speed [4,37,38] and makes the hydrogen flame stabilize closer to the burner even away from the flashback limit [21,39]. This makes the situation quite complex even for laminar premixed flames as a stretched flame burns closer to the burner surface. Predicting the flashback limits with tabulated chemistry, thus, requires a manifold which at the very least can take into account stretch induced changes in mixture fraction and changes in enthalpy due to heat transfer with the burner.

Approaches like Flamelet Progress Variable (FPV) [40,41] and Flamelet Generated Manifolds (FGM) [5,37] rely on the assumption that multi-dimensional flames are an ensemble of 1D flamelets. These flamelets can be solved using a 1D flame solver and the resulting solutions can then be stored as a function of scalars. The stored database is used to look-up flame related quantities during CFD simulation. With regards to preferential diffusion effects, Pitsch and Peters first proposed a formulation for taking into account the preferential diffusion effects in the flamelet methods [42]. Swart et al. advanced the formulation for premixed flames by analyzing the mass burning rate for hydrogen enriched flames [43] and followed this with the inclusion of preferential diffusion effects in the flamelet generated manifolds technique [10]. This was done by transporting elemental mass fractions along with the progress variable and enthalpy. This model was further advanced by tabulating for differential [9] and preferential diffusion effects [6] for hydrogen premixed flames. Another approach that takes into account differential diffusion effects for non-unity Lewis number mixtures was proposed by Regele et al. [7]. In this approach, differential diffusion was considered only in the mixture fraction transport equation and has been further modified for taking into account curvature effects [8]. Flamelet databases generated using unstrained 1D flames [44,45] and strained flames [46] have also been employed for Large Eddy Simulations. Flamelet methods have also been used for the simulation of intrinsic instabilities [47,48] by transporting the H radical along with progress variable and mixture fraction [49]. Although, great progress has been made in the field of flamelet methods with focus on hydrogen combustion, flashback limits have never been estimated with flamelet methods to the best of our knowledge and present a research gap for effective use of flamelet methods in industrial applications. Designing of hydrogen burners which offer flashback limits comparable to natural gas flames can be greatly accelerated with the help of reduced and accurate models. The challenge for the calculation of flashback limits arises from the complex interplay between stretch, stretch induced preferential diffusion effects and conjugate heat transfer between the fluid and the burner. Therefore, in this paper we follow this trajectory for the estimation of flashback limits with focus on the hydrogen flames. The objectives of this paper is to.

- Calculate the flashback limits for methane-air and hydrogen-air mixtures using the FGM approach.
- Investigate the cause for discrepancy in flashback limits calculated using detailed chemistry and FGM methods.
- Find a correction for the prediction of flashback limits without extending the dimension of the flamelet database.

The novelty of this work lies in the first time application of FGM for calculation of the flashback limits and analysis and correction of the model. We first carry out an a priori analysis using a 3D table (progress variable, enthalpy and mixture fraction) for both mixtures with flames approaching the flashback limit in Sec. FGM table generation, a priori analysis and flashback limits. Flashback limits are also estimated using CFD following the approach of Mukundakumar et al. [6]. In Sec. Analysis of over-prediction of flashback limit for hydrogen flames, we proceed to correct the source term for hydrogen flames which show over-prediction of flashback limits using default 3D FGM table by analysing their quenching behaviour. Section Conclusions concludes this study.

## Numerical model

The 2D computational model used in this study for flashback prediction comprises of a slit burner with symmetry on two sides, as shown in Fig. 1 similar to the model we have used in our recent study [3]. A premixed mixture enters at 300 K from the left with a uniform inlet velocity. On both the sides, symmetry boundary conditions are applied. Conjugate heat transfer of the fluid with the solid burner is allowed with the properties of steel with a thermal conductivity, $k = 16.7\ \mathrm{m^{-1}\,K^{-1}}$. The outlet is modelled with a Neumann type boundary condition implying that there is no change in the field variables in the normal direction. Gravitational, and viscous work effects are not modelled as they are not expected to have a major role. Radiation heat loss from the solid burner to the cold environment is modelled assuming grey body radiation with emissivity of 0.83. Chemistry of $H_2$-air flames is modelled using the mechanism of Konnov [50] which contains 15 species and 75 reactions. Methane chemistry is modelled using the DRM19 mechanism [51] which contains 21 species and 84 reactions. Constant Lewis number based mixture properties are used [52] based on conclusions from Refs. [37,53]. The constant Lewis number values are calculated by simulating one-dimensional flat flames using multi-component transport model using CHEM1D [54]. The steady equations are solved using the commercial code Ansys Fluent [55] using a coupled solver. We have used similar models and solver setting in our previous works and the reader is referred to Refs. [26,56,57] where a detailed description and validation of the numerical methods is given. An equidistant Cartesian grid with a 50 μm global grid resolution is used to solve the reacting flow equations. An additional level of grid refinement is applied in the flame zone resulting in a local resolution of 25 μm. Results showing grid independence are presented in Section A of the supplementary materials. As the flame thickness ranges from 0.3 to 0.4 mm for the lean hydrogen flames studied in this paper, the grid resolution of 25 μm is chosen such that there are enough grid points inside the flame zone.

Radiation heat loss from gas and Soret diffusion effects are ignored in the detailed chemistry simulations and the FGM database. This was done for simplicity reasons and as these two effects were found to not play a major role in the estimation of flashback limits for both fuels. From hereon, by detailed chemistry simulations we mean the solution achieved by transporting all the species in the chemical mechanism. Burner plate thickness is kept constant for both fuels while slit width and distance between slits were varied for methane and hydrogen. For $H_2$-air flames, $W = D = 1$ mm was used while for $CH_4$-air flames, $W = D = 4$ mm was used to estimate the flashback limits. This was needed as hydrogen flames are difficult to stabilize on wider burners while methane flames do not always flashback at low velocities for narrower burners. With $W = D = 1$ mm for $CH_4$-air flames, especially at low equivalence ratios, flames were found to quench by losing heat to the burner rather than flashing back. Therefore, two different burner geometries have to be used for the two fuels studied here. It is also to be noted that usage of such small opening dimensions of the burner could also possibly suppress thermo-diffusive instabilities associated with $Le < 1$ flames. Another point is that near-wall chemistry for hydrogen flames is an active field. In this study, we model the burner surface as an inert surface and simulate the correspondence between the detailed chemistry and flamelet generated manifolds solution using the same chemical mechanism.

## FGM table generation, a priori analysis and flashback limits

In this section, the basic settings and equations for 3D flamelet tables for $CH_4$-air and $H_2$-air flames are described along with a priori analysis of flashback limit flames and the difference between flashback limits calculated using the default 3D FGM and detailed chemistry. The progress variable can be defined as:

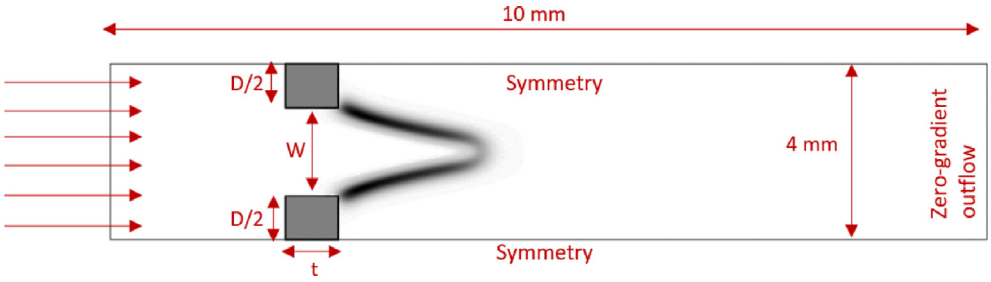


**Fig. 1 – Computational domain of the slit geometry (rotated by 90° in the clockwise direction). $W = D = 1$ mm for $H_2$-air flames and $W = D = 4$ mm for $CH_4$-air flames and $t = 0.6$ mm.**

$$Y = \sum_{i=1}^{N_s} \gamma_i Y_i. \quad (1)$$

Here, $Y_i$ are the mass fraction of species and $\gamma_i$ are the weights for each species in the progress variable. In this study, we have used $\gamma_{H_2O} = M_{H_2O}^{-1}$, $\gamma_{H_2} = -M_{H_2}^{-1}$ and $\gamma_{O_2} = -M_{O_2}^{-1}$ with $\gamma_i = 0$ for all other species for $H_2$-air mixture leading to a monotonic progress variable. In the above equations, $M_i$ is the molar mass of species i. For $CH_4$-air mixture, we have used $\gamma_{CO_2} = M_{CO_2}^{-1}$, $\gamma_{CO} = M_{CO}^{-1}$ and $\gamma_{O_2} = -M_{O_2}^{-1}$ with $\gamma_i = 0$ for all other species. The transport equations for progress variable Y, enthalpy $h$ and mixture fraction Z can be summarized as:

$$\frac{\partial}{\partial t}(\rho Z) + \nabla\cdot(\rho \mathbf{u} Z) + \nabla\cdot\left(\frac{\lambda}{c_p}\nabla\beta_Z\right) = 0, \quad (2)$$

$$\frac{\partial}{\partial t}(\rho Y) + \nabla\cdot(\rho \mathbf{u} Y) + \nabla\cdot\left(\frac{\lambda}{c_p}\nabla\beta_Y\right) = \omega_Y, \quad (3)$$

$$\frac{\partial}{\partial t}(\rho h) + \nabla\cdot(\rho \mathbf{u} h) + \nabla\cdot\left(\frac{\lambda}{c_p}\nabla T\beta_{h1} + \frac{\lambda}{c_p}\nabla\beta_{h2}\right) = 0, \quad (4)$$

where $\mathbf{u}$, $\omega_Y$, $\rho$, $\lambda$, $c_p$ and $T$ are the flow velocity vector, source term of progress variable, density, mixture conductivity, mixture specific heat capacity and temperature, respectively. For the definition of $\beta'$s in the above equation, the reader is referred to a recent publication by Mukundakumar et al. [6]. In this paper, the mixture fraction Z is defined for $H_2$-air as:

$$Z = 2\frac{Z_H}{M_H} - \frac{Z_O}{M_O} + Z_s, \quad (5)$$

with $Z_j$ being the elemental mass fractions of H and O elements and $Z_s$ is the stoichiometric mixture fraction. For $CH_4$-air mixture, mixture fraction is defined as:

$$Z = \frac{Z_C}{M_C} + 2\frac{Z_H}{M_H} - \frac{Z_O}{M_O} + Z_s, \quad (6)$$

with $Z_C$ being the elemental mass fraction of C element. The 3D databases for Y, $h$, Z are generated using flat unstretched flamelets calculated with detailed chemistry and constant Lewis numbers using CHEM1D [54] and can be summarized by the following steps.

1. Adiabatic flamelets with varying enthalpy at a constant equivalence ratio are generated by varying unburnt temperature from 300 K to 920 K.
2. Lower enthalpy flamelets are generated at the same constant equivalence ratio by diluting the unburnt mixture with $H_2O$ keeping the same $Z_H$ and $Z_O$ values at the unburnt side as found for the undiluted flamelet for hydrogen flames while 1D burner stabilized flamelets are used for methane.
3. Step 1 and 2 are repeated at equivalence ratios ranging from the lean flammability limit of 0.3 to the rich limit around 1.8 for $H_2$ and between 0.55 and 1.2 for $CH_4$-air mixtures.
4. Values of dependents (species mass fractions, transport properties etc.) are linearly extrapolated from the flamelet data towards low values of enthalpy and mixture fractions beyond the flammability limits.
5. The flamelet data is then interpolated to a rectilinear mesh in Z, $h$, Y space.

### *A priori analysis for $CH_4$-air flames*

In this subsection, an a priori analysis of methane flames near the flashback limit is provided at $\phi = 0.9$. A priori analysis is conducted by looking-up the progress variable source term from the FGM database by using the values of Y, $h$, Z from the detailed chemistry simulation results. Results for the progress variable source term $\omega_Y = \sum_{i=1}^{N_s} \gamma_i \omega_i$ from detailed chemistry simulation (DC) and from a priori lookup using the 3D flamelet table (FGM) are shown in the left and right side of Fig. 2, respectively. Flashback was found to happen at $V_{in} = 0.15$ m s$^{-1}$ and the last stable flame was found at $V_{in} = 0.175$ m s$^{-1}$. The x-axis of the plot is scaled with W = 4 mm in order to compare with results for hydrogen in the next subsection. It can be observed, that there is an overall good

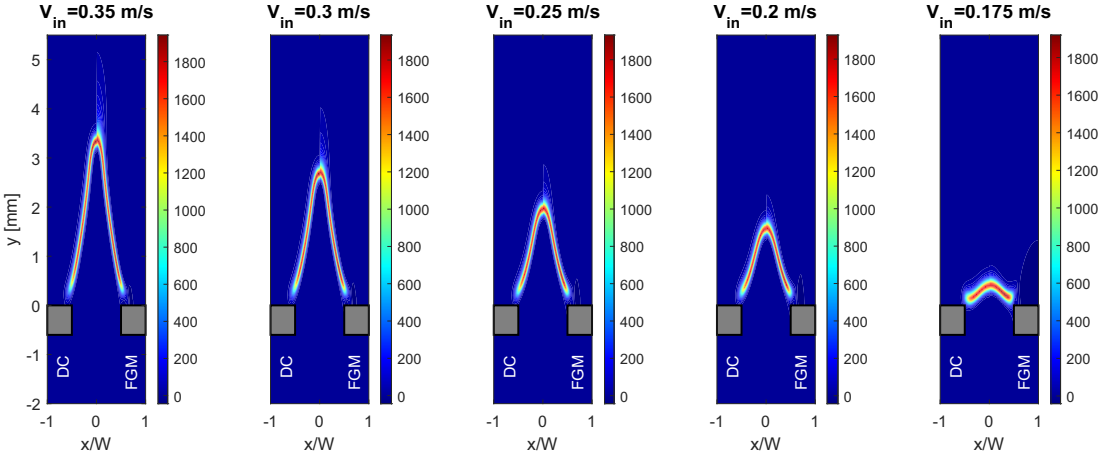


**Fig. 2 – Source term of progress variable $\omega_Y$ from detailed chemistry simulations (left side) and a priori lookup from the FGM table for $\phi = 0.9$ with decreasing flow velocity for $CH_4$-air flames. The last flame on the right, represents the flashback limit flame.**

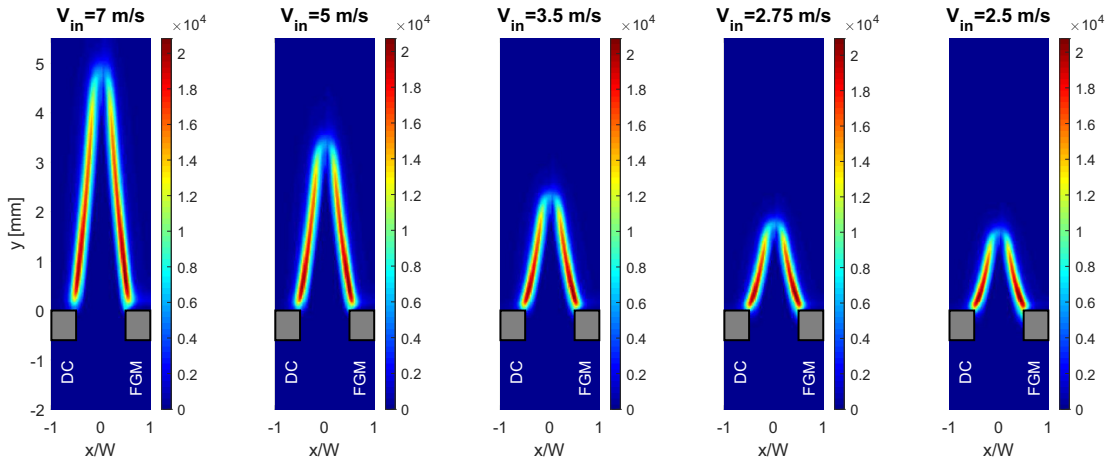


**Fig. 3 – Source term of progress variable $\omega_Y$ from detailed chemistry simulations (left side) and a priori lookup from the FGM table for $\phi = 0.7$ with decreasing flow velocity for $H_2$-air flame. The last flame on the right, represents the flashback limit flame.**

comparison between the prediction of source term from DC and FGM. A slightly thicker reaction zone can be observed at the flame tip in FGM. It can be concluded that FGM captures the source term in an accurate manner using a 3D table for $CH_4$-air flames. An a priori analysis along flamelet paths for the methane flame near the flashback limit is given in Section B of the supplementary materials.

### *A priori analysis for $H_2$-air flames*

In this subsection, an a priori analysis of the hydrogen flame approaching flashback at $\phi = 0.7$ is presented. The inlet velocity of the mixture is decreased from 7 m $s^{-1}$ in steps of 0.125 m $s^{-1}$ till flashback occurs at $V_{in} = 2.375$ m $s^{-1}$ when the flame stabilizes upstream of the burner. Results for the progress variable source term $\omega_Y$ from DC and from a priori lookup using FGM are shown in the left and right side of Fig. 3Fig. 4, respectively. It can be observed that there is good overall agreement between the detailed chemistry solution and the FGM look-up result for most of the flame sections. The source term for most of the flame sections is predicted in an excellent manner. However, near the flame base, as the flashback limit is approached at $V_{FB} = 2.5$ m $s^{-1}$, it can be observed that the source term is over-predicted on the unburnt side of the reaction zone. In order to further analyse this behaviour, 5 flame paths (labelled A to E) are reconstructed following the flame normal direction and are plotted at the flame base on top of the normalized progress variable in Fig. 4 near the flashback limit case at $V_{in} = 2.5$ m $s^{-1}$. Partially quenched flamelets A and B can be observed under the rim while the flamelets above the rim follow the progress variable from its unburnt value at 0 to burnt values around 1.

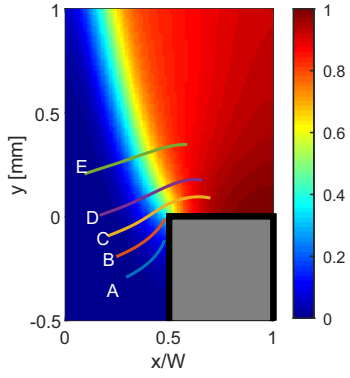


**Fig. 4 – Plot of flamelets on top of progress variable (colors) for the flashback limit case at $V_{in} = 2.5$ m $s^{-1}$ at $\phi = 0.7$ with $H_2$-air mixture, zoomed in on the flame base region. (For interpretation of the references to colour in this figure legend, the reader is referred to the Web version of this article.)**

Local profiles of $\omega_Y$, $Y_H$ and temperature $T$ are shown in Fig. 5 for the five flamelets A, B, C, D and E presented in Fig. 4. Flamelets A and B show a clear over-prediction of the source term from the flamelet database which corresponds to the over-prediction of H radical mass fraction. Temperature is however predicted well using the flamelet database. This behaviour can be hypothesized to be caused by excessive heat loss at the burnt side resulting in less production of radicals during the combustion process, which results in the source term being less than the adiabatic flamelet with $h > h_{inlet}$ included in the database. This effect needs to be included either in the table or corrected for during run time in the source term.

For flamelets C, D and E, as we move further downstream, an excellent agreement between the detailed chemistry solution and a priori FGM lookup is recovered for $\omega_Y$, $Y_H$ and $T$. This indicates that a small region near the flame base is not predicted well while just downstream of this region, a good agreement is observed. The result of this small over-prediction by FGM, however is found to play a crucial role in the prediction of flame flashback limits of $H_2$ flames. As this is a priori analysis, we can assume that the difference in source terms in Fig. 4 is not caused by the diffusion of the progress variable.

### *Flashback limits using default 3D FGM*

A comparison of flashback velocity limits $V_{FB}$ at four different equivalence ratios is shown in Fig. 6 for $CH_4$-air flames. The

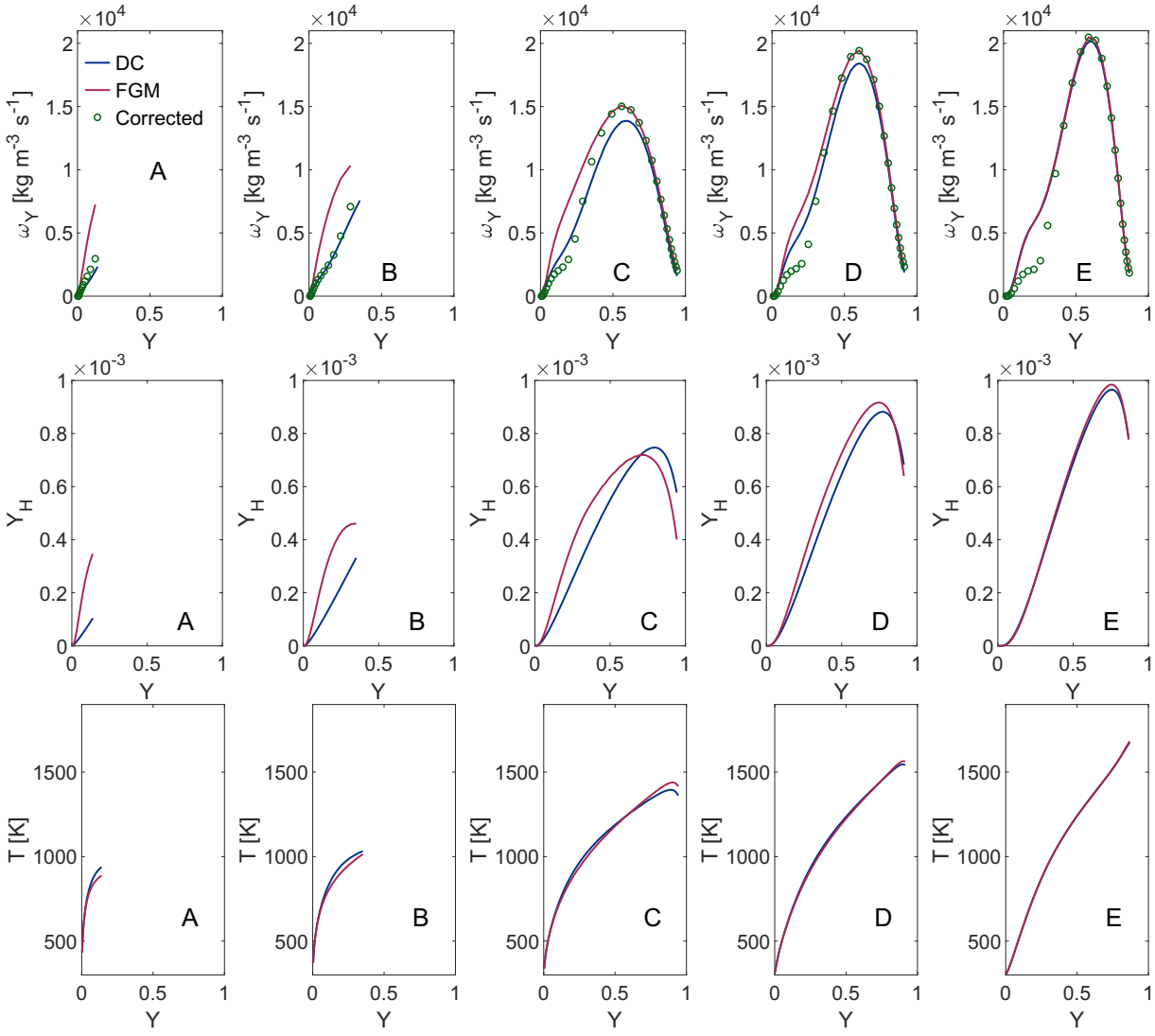


**Fig. 5 – Local profiles of $\omega_Y$, $Y_H$ and $T$ as a function of progress variable $Y$ for the five flamelets near the flame base shown in for $H_2$-air mixture. + symbols in the top plot, show the corrected source term discussed in Sec. Analysis of over-prediction of flashback limit for hydrogen flames.**

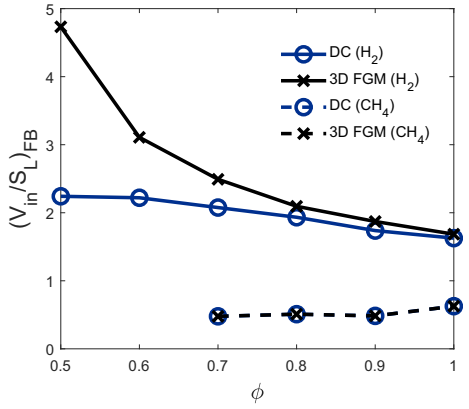


**Fig. 6 – Flashback limits scaled with the adiabatic unstretched flame speed $S_L$ for different equivalence ratios for $CH_4$-air and $H_2$-air flames.**

last stable velocity is taken as the flashback limit and is scaled with burning velocity $S_L$. It can be observed that within the limit of $V_{in} = 0.025$ m s$^{-1}$, an excellent comparison is found between the flashback limits from DC and FGM with conjugate heat transfer enabled. The flashback limits scaled with $S_L$ do not show a large variation as a function of $\phi$. This, with the help of results in Sec. A priori analysis for $CH_4$-air flames indicates that a 3D FGM is able to predict the flashback limit for methane flames in a good manner.

Flashback velocity limits $V_{FB}$ computed using different models for $H_2$-air flames are also plotted in Fig. 6 scaled with the adiabatic unstretched flame speed $S_L$ of the corresponding flat flame. Flashback limits are plotted at 6 different equivalence ratios. It can be observed that with detailed chemistry, the scaled flashback limit increases with a decrease in $\phi$. With 3D FGM (without correction), the same trend in the increasing flashback limit with decrease in $\phi$ can be observed with FGM

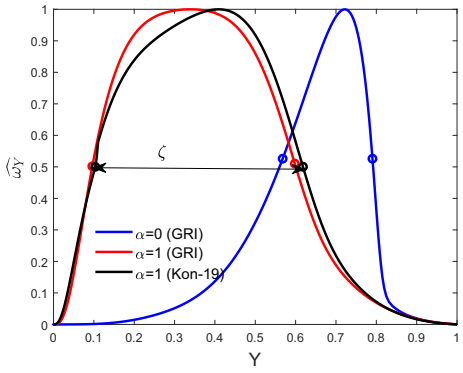


**Fig. 7 – Normalized heat released rate as a function of normalized temperature Y for stoichiometric $CH_4$-air and $H_2$-air flames.**

but the error in flashback limit prediction increases by a factor of 2 for the leanest case. It is worth mentioning here that for $\phi = 0.8, 0.9, 1$, similar behaviour with the over-prediction of $\omega_Y$ on the unburnt side was found but its impact on the flashback limits was found to be minimal. In the next section, we will present an approach for rectifying this over-prediction without the need to add any additional manifold dimension (or parameter) to the flamelet database for $H_2$-air flames.

## Analysis of over-prediction of flashback limit for hydrogen flames

In this section, an analysis into the cause of over-prediction of flashback limits using FGM for$H_2$-air flames will be conducted and a simple model for correcting the over-prediction of source term will be introduced. For this purpose, a brief discussion on the difference in reaction zone thickness of $CH_4$–$H_2$-air flames is presented in the next subsection.

### *Reaction zone thickness*

Apart from the well-known effects of higher flame speed and lower Lewis number for hydrogen than methane flames, in this subsection, we bring into focus another effect, i.e., the thickness of the reaction zone along a progress variable. For this purpose, a parameter $\zeta$ is introduced here, which is the length spanned by the source term in the progress variable space. It is defined here as the percentage of normalized progress variable value between 50% of the normalized heat release rate on the unburnt and the burnt side. Fig. 7 shows a plot of normalized heat release rate versus the scaled progress variable for stoichiometric methane and hydrogen flames (computed using the GRI 3.0 [58] for both $CH_4$-air and $H_2$-air flames, and Konnov mechanism [50] for $H_2$-air flames) using the CHEM1D code [54]. $\alpha$ is defined as $\alpha = X_{H_2}/(X_{CH_4} + X_{H_2})$ where $X_i$ is the mole fraction of species $i$ in the mixture. Here, we defined the progress variable by scaling temperature between 0 and 1. It can be seen that $\hat{\omega}$ of the $H_2$ flame occupies a larger part of progress variable than the methane flame. For hydrogen, the source term is active even at low values of progress variable. The maximum value of $\hat{\omega}$ is also shifted towards the unburnt side for $H_2$ compared to the methane flame. A brief discussion on variation of $\zeta$ for different methane and hydrogen blends is given Section C of the supplementary materials.

The thickness of the reaction zone for higher hydrogen content fuels happens as a result of diffusion of radicals O, H, OH produced during the combustion process towards the unburnt side. This enables low-temperature chemistry which makes the source term to be active in the low progress variable space for hydrogen dominated mixtures [59] as shown in Fig. 8. Due to the diffusion of radicals towards the unburnt side at low temperatures, some consumption and even production in the case of OH radicals happens [59]. The species $HO_2$ can be observed to have an active source term at very low temperatures due to the availability of major radicals. Reaction $HO_2 + OH \rightarrow H_2O + O_2$ for example, is activated at around 310 K for the presented case.

The impact of high $\zeta$ values enabled by low-temperature chemistry for $H_2$-air flames experiencing intense heat loss is the focus of the next subsection.

### *Quenching limit for $CH_4$–$H_2$-air flames*

In order to understand the effect of a thick reaction zone on flame quenching, in this subsection, a heat loss term is added to the freely propagating flame configuration in CHEM1D [54]. The heat loss term $Q_\xi = \xi(T - T_u)$ is included in the energy

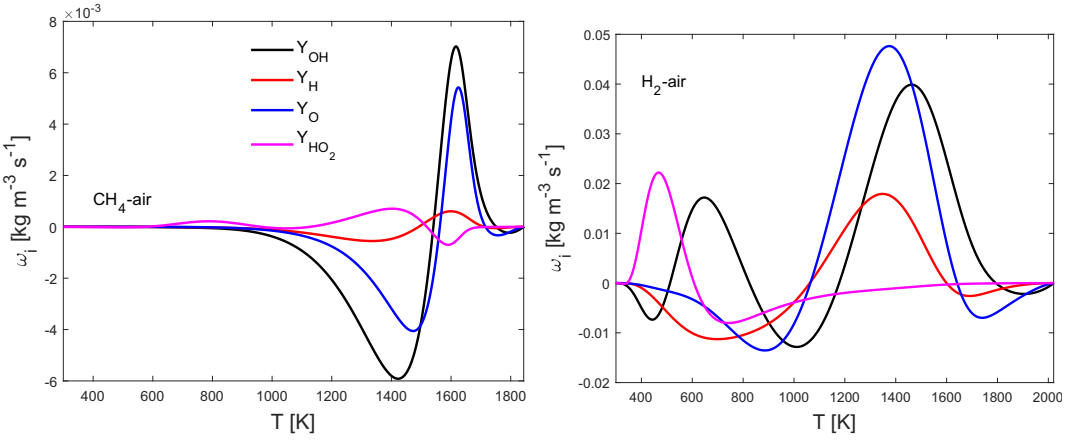


**Fig. 8 – Source term of radical as a function of temperature at $\phi = 0.7$ and $T_u = 300$ K. Top: $CH_4$-air. Bottom: $H_2$-air.**

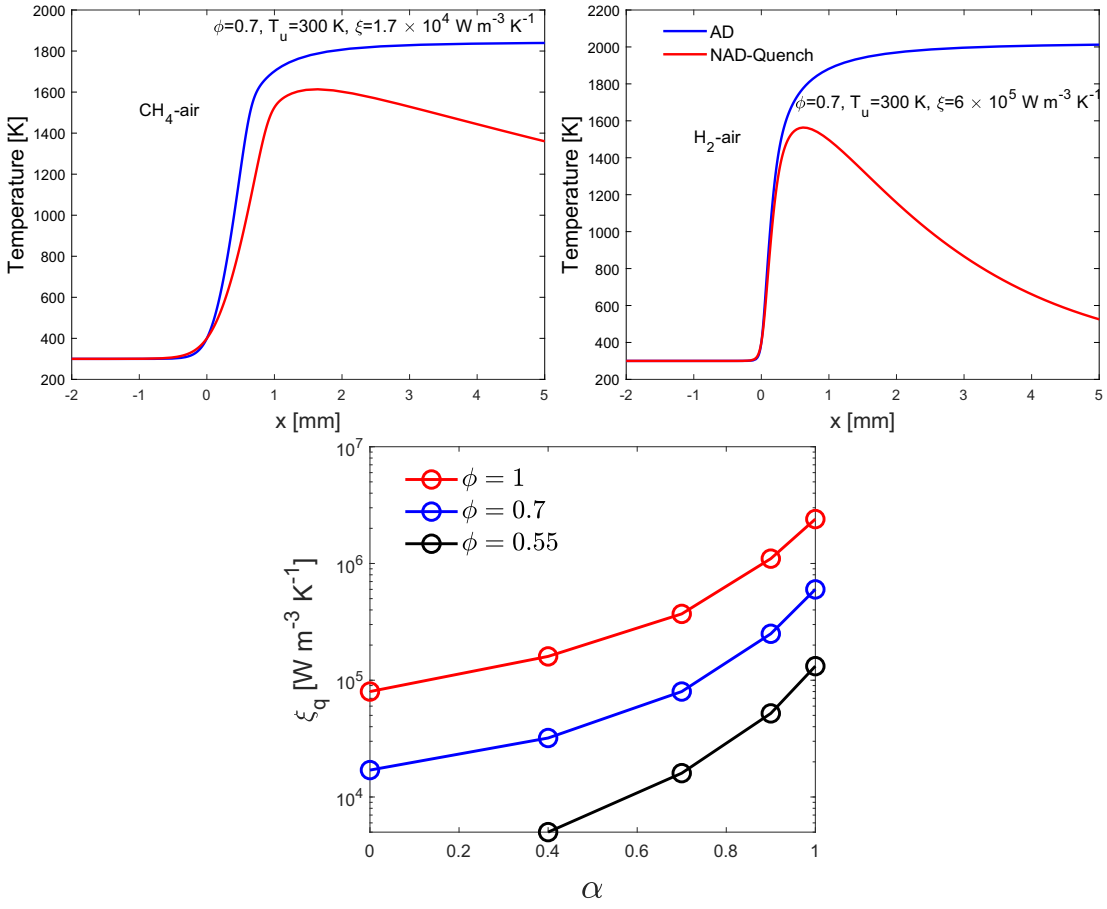


**Fig. 9 – Profiles of temperature as a function of spatial coordinate for an adiabatic flat flame (AD) and a non-adiabatic flat flame near the quenching point (NAD-Quench) for $\phi = 0.7$ and $T_u = 300$ K. Left: $CH_4$-air. Right: $H_2$-air. Bottom: Quenching limits $\xi_q$ for $CH_4$–$H_2$-air mixtures characterized by $\alpha$ at three equivalence ratios at $T_u = 300$ K using the GRI mechanism.**

equation. Here, $\xi$ is the heat transfer rate parameter with units $m^{-3}$ $K^{-1}$. Temperature profiles for $CH_4$-air and $H_2$-air flame at $T_u = 300$ K and $\phi = 0.7$ are shown in Fig. 9 near the quenching limit (labelled NAD-Quench). The quenching limit is found by increasing $\xi$ till no stable solution is found. The quenching limit for $CH_4$-air is found at $\xi = 1.7 \times 10^4$ $m^{-3}$ $K^{-1}$ while for $H_2$-air flames, it is found at $\xi = 6 \times 10^5$ $m^{-3}$ $K^{-1}$. This indicates that a hydrogen flame is able to resist quenching by an order of magnitude more than the methane flame. As a reference, adiabatic results are also plotted in Fig. 9 (labelled AD). For the $CH_4$-air flame, the maximum flame temperature can be observed to be lower than the adiabatic flame temperature due to heat losses. For the $H_2$ flame, it can be observed that the maximum value of temperature is greatly reduced but still high enough to sustain the production and transport of radicals. At x = 5 mm, the temperature is almost reduced to the specified value $T_u$, much lower than that for the methane flame.

Quenching limits $\xi_q$ for different mixtures of $CH_4$–$H_2$-air are also plotted in Fig. 9 at three equivalence ratios and at $T_u = 300$ K. We can observe that at higher $\phi$, quenching occurs at higher values of $\xi$. The major observation from Fig. 9 is that as $\alpha$ is increased (which also increases reaction zone thickness $\zeta$), the quenching limits increase exponentially at all three equivalence ratios. This indicates the strong impact, a low-temperature chemistry enabled thick reaction zone has on resisting quenching. Therefore, we can hypothesize that because the methane flame quenches at lower $\xi$ values than the hydrogen flame, the effect of a thick reaction zone subjected to intensive heat loss could be less important in methane flames.

### *A simple model for source term correction*

In this section, based on the analysis presented above, we aim to introduce a correction factor model which can adjust the source term for hydrogen flames without the need for extending the dimension of the FGM table. Here, it should be mentioned that the need for extending the dimension of the FGM table or for the development of a model for source term correction which could substitute such an extension arises due to.

1. The absence of strong enthalpy gradients across the reaction zone in the flamelet database.
2. Such strong enthalpy gradients which are present in the multi-slit flames simulated with detailed chemistry (transported species) across a thick reaction zone for $H_2$-air flames result in the reduction of the source term when compared to the flamelet database.

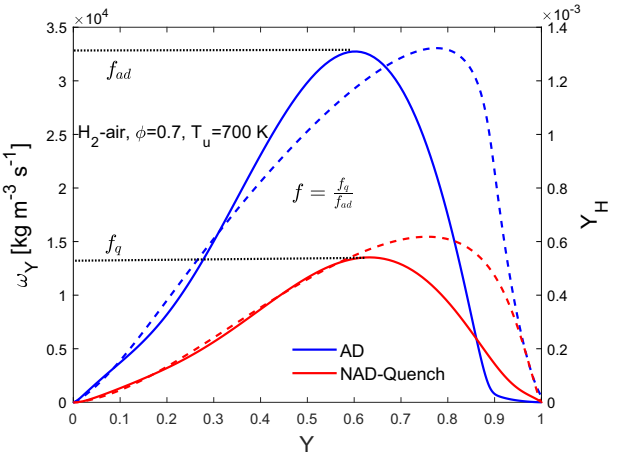


**Fig. 10 – Top: Profiles of source term $\omega_Y$ (solid) and hydrogen radical mass fraction $Y_H$ (dashed) for adiabatic flat flame and non-adiabatic flat flame near the quenching point for $H_2$-air flame at $\phi = 0.7$ and $T_u = 700$ K using the Konnov mechanism.**

3. As presented in the previous subsection, if a heat sink term is included across the thick reaction zone, we can qualitatively capture this effect of source term reduction which is quite dominant for the $H_2$-air flames.

In order to develop a simple model which can quantitatively correct the source term of the progress variable, the source term and H radical mass fraction are shown in Fig. 10 for the quenching case at a higher value of $T_u$ than the one present in Fig. 9. It can be clearly observed that $\omega_Y$ reduces due to heat loss and the accompanying depletion of H radical can also be observed. This decrease in the source term is crucial to be included in the FGM framework especially on the unburnt side of flame reaction zone as larger discrepancies were observed in Fig. 5 there. The source term on the unburnt side can be assumed to be a linear function of Y from the 1D simulations and as such the difference between the quenched and the adiabatic simulation on the unburnt side can be correlated only with the slope of this line. In order to include this information in the FGM source term, we introduce a correction factor $f$ as

$$f = \frac{f_q}{f_{ad}}, \tag{7}$$

where $f_{ad}$ is the value of the maximum source term for the adiabatic flamelet while $f_q$ is the value of the maximum source term for the non-adiabatic flamelet near the quenching limit as also illustrated in Fig. 10. Here, we make an assumption that the correction factor $f$ for the source term at the prescribed $T_u$ value corresponds to the local $T$ along the flamelet. In this way, the local value of $\omega_Y$ as a function of local gas temperature can be corrected by correcting the slope of the $\omega_Y$-Y space. The factor $f$ is then collected for various unburnt gas temperatures and used to fit a 2nd degree polynomial between 300 K and 850 K for each equivalence ratio as

$$f^* = a_0 + a_1 T + a_2 T^2. \tag{8}$$

**Table 1 – Coefficients used to fit quenching limits as a function of temperature.**

| $\phi$ | $a_0$ | $a_1 \times 10^{-3}$ | $a_2 \times 10^{-6}$ |
|---|---|---|---|
| 1 | 0.49 | 0.43 | −0.61 |
| 0.9 | 0.46 | 0.47 | −0.62 |
| 0.8 | 0.54 | 0.34 | −0.61 |
| 0.7 | 0.44 | 0.42 | −0.7 |
| 0.6 | 0.37 | 0.32 | −0.77 |
| 0.5 | 0.30 | 1.15 | −1.36 |

The values of coefficients in above equation are given in Table 1 for 6 equivalence ratios of $H_2$-air flames. Beyond 850 K, a smoothing function is used to transition the correction factor to the value of 1 at around 1000 K. This smoothing factor is calculated as

$$S = 0.5\tanh\left(\frac{T-1000}{50}\right) + 0.5. \tag{9}$$

The final correction factor F for the source term then reads

$$F = \frac{\omega_Y^*}{\omega_Y} = S + (1-S)f^*, \tag{10}$$

The source term correction factor F is shown in Fig. 11 for $\phi = 0.7$. The values of $f$ from 1D simulations are plotted with circles at different $T_u$'s while the fitted and smoothed function F is plotted as a solid line. Some scatter can be observed in values of $f$ at low temperature values due to slight inaccuracy in the calculation of the quenching limit. Overall, it can be observed that the correction factor decreases with increasing temperature. A comparison with a priori lookup is plotted in Fig. 5 with ∘ symbols for the source term in the $\omega_Y$ plots where the source term is corrected as $\omega_Y^* = F\omega_Y$ as a function of local temperature $T$. It can be observed that the comparison is significantly improved compared to the default look-up especially for flamelet A and B. A slight under-prediction occurs for flamelets D and E but this under-prediction is much smaller compared to the integrated source term over the flamelet. The good comparison at the most upstream

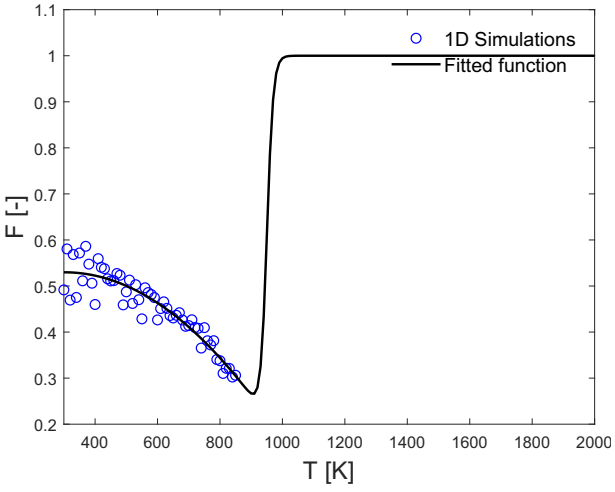


**Fig. 11 – Variation of source term correction factor F as a function of temperature for $H_2$-air mixture at $\phi = 0.7$.**

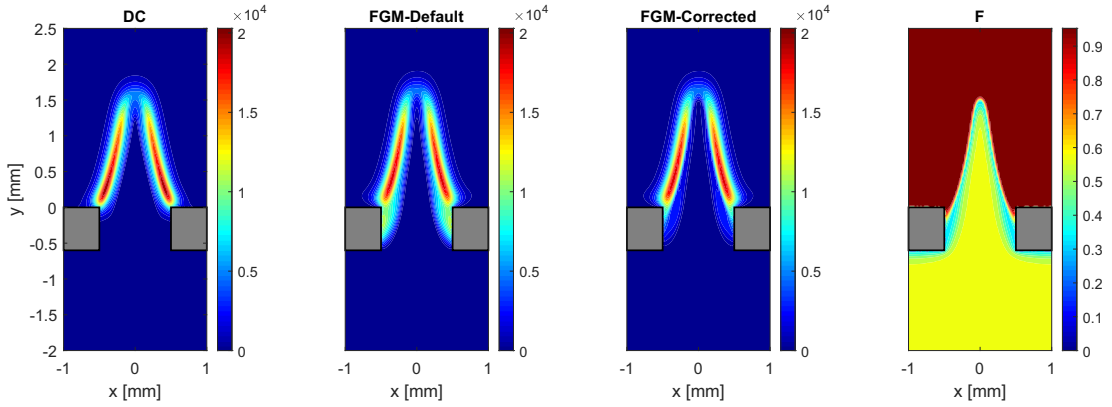


**Fig. 12 – Top: Source term $\omega_Y$ using detailed chemistry (DC), default FGM (FGM-Default) and FGM with corrected source term (FGM-Corrected) and the correction factor F for $H_2$-air flame at $\phi = 0.7$ at $V_{in} = 2.5$ m $s^{-1}$.**

flamelets gives credibility to the applied procedure and in the next subsection, the source term is corrected at run-time in the CFD simulations and flashback limits are re-calculated for the same cases. As we have used 1D flames with no geometrical restrictions for the calculation of the correction factor $f^*$, we believe that these coefficients can give satisfactory results for a wide variety of geometrical configurations.

### *Flashback limits calculated using corrected source term*

The flashback limit flames computed with uncorrected and corrected source term along with the factor $F$ are shown in Fig. 12 for $\phi = 0.7$ at $V_{in} = 2.5$ m $s^{-1}$. In comparison to the a priori result in Fig. 3, the solution shows stronger burning in the slit. This possibly happens due to the fact that the a priori analysis assumes that the control variables will remain the same as in detailed chemistry simulation. However, this is not the case here, as the flame can move further upstream and increase the burner temperature, thus, resulting in a higher source term at the unburnt side. The results with the corrected source term show that this higher increase in source term is limited by the application of the correction factor which reduces the source term in the critical flame base region. Despite this, there is still some over-prediction in the FGM-Corrected source term. The plot of $F$ shows the variation of this correction factor as a 2D field and it can be observed to have lower values near the inner sides of the burner. A comparison of progress variable, enthalpy and mixture fraction results from detailed chemistry and FGM is included in the Section D of the supplementary materials.

The flashback velocity limits predicted with source term correction are plotted in Fig. 13 along with the results from detailed chemistry and from FGM without source term correction. It can be observed that the flashback limits now are in a good agreement with those calculated from detailed chemistry simulations within the margin of flashback limit error (0.125 m $s^{-1}$). This confirms the impact of the thick reaction zone near the flame base where conjugate heat transfer with the burner greatly influences the progress variable source term. Inclusion of this effect using a systematic and simple approach appears to solve the problem of flame flashback prediction.

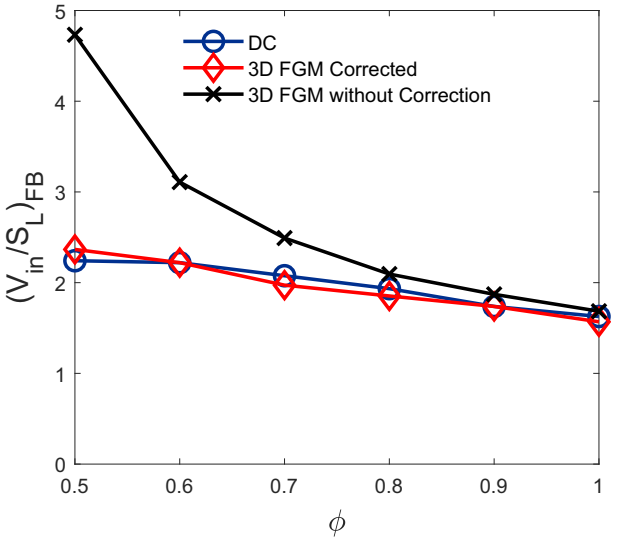


**Fig. 13 – Flashback limits scaled with the adiabatic unstretched flame speed $S_L$ for different equivalence ratios for $H_2$-air flames.**

## Conclusions

In this study, we have successfully tested the flamelet generated manifold method for the estimation of flame flashback limits for $H_2$-air flames stabilized on a slit burner. It is found that a 3D manifold can predict the flashback limits for $CH_4$-air flames in an adequate manner. On the other hand, a 3D manifold by itself cannot predict the impact of enthalpy gradients on the thick reaction zone for $H_2$-air flames. This effect has a noticeable effect on the flashback limits calculated using FGM with conjugate heat transfer especially at lower equivalence ratios. The problem can be corrected, at least for the flashback limit calculation, by adding a correction factor to the source term. This correction factor can be estimated using 1D flamelets with the addition of a heat loss term. In the end, it is found that the flashback limits calculated with a source term corrected FGM table, compare well with those calculated with detailed chemistry simulations.

## Declaration of competing interest

The authors declare that they have no known competing financial interests or personal relationships that could have appeared to influence the work reported in this paper.

## Acknowledgements

This work has been sponsored by Simon Steven Meester award (STW-11995) to prof. Dr. L. P. H. de Goey from the Netherlands Organisation for Scientific Research (NWO). Additional financial and technical support from Polidoro S. p.A. and Ferroli S. p.A. is gratefully acknowledged.

## Appendix A. Supplementary data

Supplementary data to this article can be found online at https://doi.org/10.1016/j.ijhydene.2023.03.262.

## REFERENCES

[1] Jiménez C, Fernández-Galisteo D, Kurdyumov VN. DNS study of the propagation and flashback conditions of lean hydrogen-air flames in narrow channels: symmetric and non-symmetric solutions. Int J Hydrogen Energy 2015;40(36):12541–9.
[2] Aniello A, Poinsot T, Selle L, Schuller T. Hydrogen substitution of natural-gas in premixed burners and implications for blow-off and flashback limits. Int J Hydrogen Energy 2022;47(77):33067–81.
[3] Vance F, de Goey L, van Oijen J. Development of a flashback correlation for burner-stabilized hydrogen-air premixed flames. Combust Flame 2022;243:112045.
[4] Law CK. Dynamics of stretched flames. Symp (Int) Combust 1989;22:1381–402.
[5] van Oijen J, de Goey LPH. Modelling of premixed laminar flames using flamelet-generated manifolds. Combust Sci Technol 2007;161:113–37.
[6] Mukundakumar N, Efimov D, Beishuizen N, van Oijen J. A new preferential diffusion model applied to FGM simulations of hydrogen flames. Combust Theor Model 2021;25(7):1245–67.
[7] Regele JD, Knudsen E, Pitsch H, Blanquart G. A two-equation model for non-unity Lewis number differential diffusion in lean premixed laminar flames. Combust Flame 2013;160:240–50.
[8] Schlup J, Blanquart G. Reproducing curvature effects due to differential diffusion in tabulated chemistry for premixed flames. Proc Combust Inst 2019;37:2511–8.
[9] Donini A, Bastiaans R, van Oijen J, de Goey L. Differential diffusion effects inclusion with flamelet generated manifold for the modeling of stratified premixed cooled flames. Proc Combust Inst 2015;35:831–7.
[10] de Swart J, Bastiaans R, van Oijen J, de Goey L, Cant R. Inclusion of preferential diffusion in simulations of premixed combustion of hydrogen/methane mixtures with flamelet generated manifolds, flow turbul. Combust 2010;85:473–511.
[11] Ranga Dinesh K, Jiang X, van Oijen J. Numerical simulation of hydrogen impinging jet flame using flamelet generated manifold reduction. Int J Hydrogen Energy 2012;37(5):4502–15.
[12] Luo Y, Ferraro F, Breicher A, Böttler H, Dreizler A, Geyer D, Hasse C, Scholtissek A. A novel flamelet manifold parametrization approach for lean CH4–H2-air flames. Int J Hydrogen Energy 2023;48(1):407–21. ISSN 0360-3199.
[13] Vreman A, van Oijen J, de Goey L, Bastiaans R. Direct numerical simulation of hydrogen addition in turbulent premixed Bunsen flames using flamelet-generated manifold reduction. Int J Hydrogen Energy 2009;34(6):2778–88.
[14] Shan F, Hou L, Chen Z, Chen J, Wang L. Linearized correction to a flamelet-based model for hydrogen-fueled supersonic combustion. Int J Hydrogen Energy 2017;42(16):11937–44.
[15] Liu X, Shao W, Liu C, Bi X, Liu Y, Xiao Y. Numerical study of a high-hydrogen micromix model burner using flamelet-generated manifold. Int J Hydrogen Energy 2021;46(39):20750–64.
[16] Almutairi F, Dinesh KR, van Oijen J. Modelling of hydrogen-blended dual-fuel combustion using flamelet-generated manifold and preferential diffusion effects. Int J Hydrogen Energy 2023;48(4):1602–24.
[17] Zhang W, Wang J, Lin W, Mao R, Xia H, Zhang M, Huang Z. Effect of differential diffusion on turbulent lean premixed hydrogen enriched flames through structure analysis. Int J Hydrogen Energy 2020;45(18):10920–31. ISSN 0360-3199.
[18] Kai R, Tokuoka T, Nagao J, Pillai AL, Kurose R. LES flamelet modeling of hydrogen combustion considering preferential diffusion effect. Int J Hydrogen Energy 2023;48(29):11086–101.
[19] Lipatnikov AN, Sabelnikov VA. An extended flamelet-based presumed probability density function for predicting mean concentrations of various species in premixed turbulent flames. Int J Hydrogen Energy 2020;45(55):31162–78. ISSN 0360-3199.
[20] Altay H, Kedia K, Speth R, Ghoniem A. Two-dimensional simulations of steady perforated-plate stabilized premixed flames. Combust Theor Model 2010;14(1):125–54.
[21] Vance F, Shoshin Y, de Goey L, van Oijen J. Quantifying the impact of heat loss, stretch and preferential diffusion effects to the anchoring of bluff body stabilized premixed flames. Combust Flame 2022;237:111729.
[22] Shoshin Y, Bastiaans R, de Goey LPH. Anomalous blow-off behavior of laminar inverted flames of ultra-lean hydrogen–methane–air mixtures. Combust Flame 2013;160:565–76.
[23] Berger S, Duchaine F, Gicquel LYM. Bluff-body thermal property and initial state effects on a laminar premixed flame anchoring pattern. Flow, Turbul Combust 2018;100:561–91.
[24] Kedia KS, Ghoniem AF. The anchoring mechanism of a bluff-body stabilized laminar premixed flame. Combust Flame 2014;161:2327–39.
[25] Miguel-Brebion M, Mejia D, Xavier P, Duchaine F, Bedat B, Selle L, Poinsot T. Joint experimental and numerical study of the influence of flame holder temperature on the stabilization of a laminar methane flame on a cylinder. Combust Flame 2016;172:153–61.
[26] Vance FH, Shoshin Y, Goey LPH, van Oijen JA. An investigation into flashback and blow-off for premixed flames stabilized without a recirculation vortex. Combust Flame 2022;235:111690.
[27] Kedia KS, Ghoniem AF. The blow-off mechanism of a bluff-body stabilized laminar premixed flame. Combust Flame 2015;162:1304–15.
[28] Li D, Wang R, Yang G, Wan J. Effect of hydrogen addition on the structure and stabilization of a micro-jet methane diffusion flame. Int J Hydrogen Energy 2021;46(7):5790–8.

[29] Wan J, Zhao H. Anomalous blow-off behavior of a holder-stabilized premixed flame in a preheated mesoscale combustor. Combust Flame 2021;230:111452.
[30] Boeck L, Lapointe S, Melguizo-Gavilanes J, Ciccarelli G. Flame propagation across an obstacle: OH-PLIF and 2-D simulations with detailed chemistry. Proc Combust Inst 2017;36(2):2799–806.
[31] Melguizo-Gavilanes J, Bauwens L. Shock initiated ignition for hydrogen mixtures of different concentrations. Int J Hydrogen Energy 2013;38(19):8061–7.
[32] Pers H, Aniello A, Morisseau F, Schuller T. Autoignition-induced flashback in hydrogen-enriched laminar premixed burners. Int J Hydrogen Energy 2023;48(27):10235–49.
[33] Kıymaz TB, Böncü E, Güleryüz D, Karaca M, Yılmaz B, Allouis C, Gökalp İskender. Numerical investigations on flashback dynamics of premixed methane-hydrogen-air laminar flames. Int J Hydrogen Energy 2022;47(59):25022–33. ISSN 0360-3199.
[34] Reichel TG, Paschereit CO. Interaction mechanisms of fuel momentum with flashback limits in lean-premixed combustion of hydrogen. Int J Hydrogen Energy 2017;42(7):4518–29. ISSN 0360-3199.
[35] Xie Y, Qin C, Chen Z, Duan P, Guo S. The impact of hydrogen addition to natural gas on flame stability. Int J Hydrogen Energy 2022;47(84):35851–63. ISSN 0360-3199.
[36] Xia H, Han W, Wei X, Zhang M, Wang J, Huang Z, et al. Numerical investigation of boundary layer flashback of CH4/H2/air swirl flames under different thermal boundary conditions in a bluff-body swirl burner. Proc Combust Inst 2023;39(4):4541–51.
[37] van Oijen JA, Donini A, Bastiaans RJM, ten thije Boonkkamp JHM, de Goey LPH. State-of-the-art in premixed combustion modeling using flamelet generated manifolds. Prog Energy Combust Sci 2016;57:30–74.
[38] Giannakopoulos GK, Gatzoulis A, Frouzakis CE, Matalon M, Tomboulides AG. Consistent definitions of "flame displacement speed" and "markstein length" for premixed flame propagation. Combust Flame 2015;162:1249–64.
[39] Michaels D, Shanbhogue SJ, Ghoniem AF. The impact of reactants composition and temperature on the flow structure in a wake stabilized laminar lean premixed CH4/H2/air flames; mechanism and scaling. Combust Flame 2017;176:151–61.
[40] Ihme M, Pitsch H. Modeling of radiation and nitric oxide formation in turbulent nonpremixed flames using a flamelet/progress variable formulation. Phys Fluids 2008;20(5):055110.
[41] Pierce CD, Moin P. Progress-variable approach for large-eddy simulation of non-premixed turbulent combustion. J Fluid Mech 2004;504:73–97.
[42] Pitsch H, Peters N. A consistent flamelet formulation for non-premixed combustion considering differential diffusion effects. Combust Flame 1998;114(1):26–40. ISSN 0010-2180.
[43] de Swart JAM, Groot GRA, van Oijen JA, de Goey LPH, ten Thije Boonkkamp JHM. Detailed analysis of the mass burning rate of stretched flames including preferential diffusion effects. Combust Flame 2006;145:245–58.
[44] Langella I, Swaminathan N, Pitz RW. Application of unstrained flamelet SGS closure for multi-regime premixed combustion. Combust Flame 2016;173:161–78.
[45] Chen ZX, Langella I, Barlow RS, Swaminathan N. Prediction of local extinctions in piloted jet flames with inhomogeneous inlets using unstrained flamelets. Combust Flame 2020;212:415–32.
[46] Trisjono P, Kleinheinz K, Hawkes ER, Pitsch H. Modeling turbulence–chemistry interaction in lean premixed hydrogen flames with a strained flamelet model. Combust Flame 2016;174:194–207. ISSN 0010-2180.
[47] Wen X, Zirwes T, Scholtissek A, Böttler H, Zhang F, Bockhorn H, et al. Flame structure analysis and composition space modeling of thermodiffusively unstable premixed hydrogen flames — Part I: atmospheric pressure. Combust Flame 2022;238:111815.
[48] Böttler H, Lulic H, Steinhausen M, Wen X, Hasse C, Scholtissek A. Flamelet modeling of thermo-diffusively unstable hydrogen-air flames. Proc Combust Inst 2023;39(2):1567–76.
[49] Knudsen E, Kolla H, Hawkes ER, Pitsch H. LES of a premixed jet flame DNS using a strained flamelet model. Combust Flame 2013;160(12):2911–27. ISSN 0010-2180.
[50] Konnov A. Yet another kinetic mechanism for hydrogen combustion. Combust Flame 2019;203:14–22.
[51] Kazakov A, Frenklach M. Reduced reaction sets based on GRI-mech 1.2 URL. http://combustion.berkeley.edu/drm/.
[52] Smooke MD, Giovangigli V. Reduced reaction sets based on GRI-mech 1.2. Springer Verlag; 1991.
[53] Burali N, Lapointe S, Bobbitt B, Blanquart G, Xuan Y. Assessment of the constant non-unity Lewis number assumption in chemically-reacting flows, Combust. Theory Mod 2016;20:632–57.
[54] A One dimensional laminar flame code. Eindhoven University of Technology; 2023.
[55] Ansys® Fluent, Release 19.2, 2021.
[56] Vance FH, Shoshin Y, van Oijen JA, Goey LPH. Effect of Lewis number on premixed laminar lean-limit flames stabilized on a bluff body. Proc Combust Inst 2019;37(2):1663–72.
[57] Vance FH, Shoshin Y, de Goey LPH, van Oijen JA. Flame stabilization regimes for premixed flames anchored behind cylindrical flame holders. Proc Combust Inst 2021;38:1983–92.
[58] Smith GP, Golden DM, Frenklach M, Moriarty NW, Eiteneer B, Goldenberg M, Bowman CT, Hanson RK, Song S, Gardiner WC, Jr., Lissianski VV, Qin Z, GRI 3.0 1995.
[59] Law CK. Combustion physics. New York: Cambridge University Press; 2006.